In-vitro corrosion performance of hydroxyapatite-coated Al2024 in simulated body fluid: A comparative study

Hidroksiapatit kaplanmış Al2024'ün simüle edilmiş vücut sıvısında *in-vitro* korozyon performansı: Karşılaştırmalı bir çalışma

Mehmet Topuz[1],* 🆔, **Burak Dikici[2]** 🆔

[1] *Van Yüzüncü Yıl University, Mechanical Engineering Department, 65080, Van, Türkiye*
[2] *Atatürk University, Metallurgical and Materials Engineering Department, 25240, Erzurum, Türkiye*

Abstract

In this study, the applicability of hydroxyapatite (HA) coatings on Al-Cu-Mg alloys (Al2024) was investigated by electrochemical techniques. The structural characterizations of the coated layers were investigated by SEM, EDS, and XRD equipment. The surface adhesion resistance and electrochemical degradation behavior were tested by scratch and potentiodynamic scanning (PDS) tests, respectively. It was observed that the HA coating had a homogeneous structure on the Al2024 surfaces, but some local areas could not be adequately coated with HA from the cross-section images. Also, the coating surfaces were microporous morphology, which is specific to the HA coatings. From the scratch test results of the coating, it was predicted that the critical load resistance (L_{c1}), 12N, would be sufficient for biomedical applications. Electrochemical corrosion tests revealed that HA coating decreased the corrosion current density (I_{corr}) and corrosion rate of the Al2024 alloy (0.885 and 5.260 µA·cm^{-2} for HA-coated and uncoated Al2024 alloy, respectively). However, despite the low I_{corr} value obtained with HA coating, it was observed that both I_{corr} and passivation current density (I_{pass}) values (3.15 µA·cm^{-2} for HA coating, 0.03 to 0.08 µA·cm^{-2} for different types of titanium alloys) were insufficient when compared to commercial titanium alloys.

Keywords: Al2024, Hydroxyapatite, Implant, Simulated body fluid, Sol-gel coating

Öz

Bu çalışmada, hidroksiapatit (HA) kaplamaların Al-Cu-Mg alaşımları (Al2024) üzerine uygulanabilirliği elektrokimyasal tekniklerle incelenmiştir. Kaplanan tabakaların yapısal karakterizasyonları SEM, EDS ve XRD test/analizleri ile incelenmiştir. Yüzey adezyon direnci ve elektrokimyasal bozunma davranışı, sırasıyla çizilme ve potansiyodinamik tarama (PDS) testleri ile test edilmiştir. Al2024 yüzeylerinde HA kaplamanın homojen bir yapıya sahip olduğu ancak kesit görüntülerinden bazı lokal bölgelerin yeterince HA ile kaplanamadığı görülmüştür. Ayrıca kaplama yüzeyleri, HA kaplamalara özgü mikro gözenekli morfolojiye sahip olduğu tespit edilmiştir. Kaplamanın çizilme testi sonuçlarından, kritik yük direncinin (L_{c1}), 12N'un biyomedikal uygulamalar için yeterli olacağı öngörülmüştür. Elektrokimyasal korozyon testleri, HA kaplamanın Al2024 alaşımının korozyon akımı yoğunluğunu (I_{corr}) ve korozyon oranını azalttığını ortaya çıkarmıştır (HA kaplı ve kaplanmamış Al2024 alaşımı için sırasıyla 0,885 ve 5,260 µA·cm^{-2}). Ancak HA kaplama ile elde edilen düşük I_{corr} değerine rağmen hem I_{corr} hem de pasivasyon akım yoğunluğu (I_{pass}) değerlerinin (HA kaplama için 3,15 µA·cm^{-2}, farklı titanyum türleri için 0.03 ila 0.08 µA·cm^{-2}) olduğu gözlemlenmiş olup ticari titanyum alaşımlarına kıyasla yetersiz olduğu ortaya çıkarılmıştır.

Anahtar kelimeler: Al2024, Hidroksiapatit, İmplant, Simüle edilmiş vücut sıvısı, Sol-jel kaplama

1 Introduction

316L stainless steel, cobalt and chromium alloys, and titanium (Ti) and its alloys are frequently used due to their unique properties compared to other implant materials in medical applications [1, 2]. Among these metallic materials, titanium and its alloys are distinguished from other metallic implant materials because of their enhanced toughness, strength, Young's modulus, bio-integration, and corrosion resistance [1, 3, 4]. The first property of a material used as an implant is biocompatibility, followed by a low Young's modulus. Young's modulus of biomedical material has a considerable designation with the term "Wolff's law, also known as "stress-shielding effect" explained with bone in a

healthy person, which regenerates itself in response to the loads on its [5]. In terms of Wolff's law which refers to the density reduction of bone as a result of all stress to implant material rather than to the bone [4]. The distribution of the load over both bone and implant material is closely related to the elastic modulus of the material used as an implant material. In this way, although the specific strength values [6] of these commercially used alloys are high, the elastic modulus of Ti alloys (100 – 120 GPa) [7] is still higher than cortical bone (15 – 30 MPa) [8]. On the other hand, it is required that an implant material that is considered for biomedical application should have both anti–toxic and anti-

allergic properties. Besides, it is required to have a low elastic modulus by Wolff's Law mentioned above [9].

Apart from these features expected from biomaterials must be accessible according to the welfare level of people. Aluminum is the third most common element in nature. On the other hand, 100 Mt (million metric tons) of aluminum is produced annually, and approximately 75% is scrapped. Therefore, it comes to mind that such a large amount of elements can be used as a biomaterial and can be a cost-effective solution in implant applications [10]. On the other hand, compared to pure aluminum, especially 2XXX series aluminum alloys have advanced properties such as secondary strength because they can be solution heat-treated and artificially aged (CuAl$_2$) due to Cu (2.5 – 5.0%) contained in aluminum alloys [11]. However, there are only limited attempts on Al-based alloys usage of their as biomaterials in the literature due to their insufficient biocompatibility properties [12–14].

A biomaterial used as an implant material is highly associated with its surface properties and compatibility with the surrounding tissues. When a biomaterial is used directly in the body, surrounding tissues recognize it as a foreign matter, and some unwanted reaction will occur at the biomaterial tissue interface. Breme et al. [15] describe these unwanted reactions briefly; *i)* metal ions flow to the tissues, resulting in corrosion, *ii)* toxicity exceeds the amount of metal ions in tissue, *iii)* metal ions react with proteins and convert to allergy or inflammation and *iv)* production of H$_2$O$_2$ by inflammatory cells. These unwanted reactions could be prevented by coating the surface with bioactive elements so that the tissue will recognize the implant material and cause any unwanted reaction, as it's known that bone structure mostly consists of calcium (Ca) and phosphate (P). Hydroxyapatite (Ca$_{10}$(PO$_4$)$_6$(OH)$_2$: HA) is most similar to the bone structure due to the stoichiometric ratio of Ca and P elements in its chemical structure, and this ratio gives it high stability [16–18]. The artificially synthesized HA suffers from its low mechanical (fatigue and toughness) properties, so its use by itself is limited [19, 20].

On the other hand, HA is commonly used as a coating material on varied metallic surfaces. However, the use of HA as a sole coating material is limited and can be explained as follows; *i)* crystal structure difference between implant and coatings interfaces (metallic–ceramic crystal structure) [21] and *ii)* low mechanical properties such as high brittleness, weak tensile and fatigue strength, and wear resistance [22, 23]. However, hydroxyapatite can be used to fulfill various functions in materials that are mostly integrated with biological systems due to their properties, such as bioactivity [22], osteoconductivity [24], and biocompatibility [25].

Recently, many methods have been commercially used for synthesizing bioactive coatings on metallic materials, such as plasma spray [26], magnetron sputtering [27], electrochemical deposition [28], and sol-gel [22]. The method used in synthesizing bioactive coatings should be selected considering the thickness, surface roughness, crystallinity, equipment price, and safety. Therefore, the sol-gel-derived dip coating method is notable among the other coating methods because not dependent on the shape; high purity and homogeneity can be obtained at a low cost [29].

In this study, HA coatings were deposited by the sol-gel method on Al2024 alloy for possible applications in biomedical fields. Microstructural, mechanical, and *in-vitro* electrochemical corrosion properties of coatings were discussed in detail.

2 Material and methods

2.1 Sol-gel coating process

Before the coating process, the surfaces were sandblasted with 250µm Al$_2$O$_3$ powders under 6 bar pressures for the coatings to adhere tightly to the surface of 10×20mm Al2024 substrates. The chemical composition of Al2024 was 4.35% Cu, 0.5% Fe, 1.5% Mg, 0.6% Mn, 0.5% Si, and 0.25% Zn, and the remained (92.3%) was Al by weight. After the sandblasting process, surface cleaning was carried out in ethyl alcohol and ethanol for 5min to degrease the Al$_2$O$_3$ particles adhered by the plastic deformation on the surface. Distilled water (DW), ammonia, calcium nitrate tetrahydrate (Ca(NO$_3$)$_2$·4H$_2$O), and diammonium hydrogen phosphate ((NH$_4$)$_2$HPO$_4$) (Merck) have been used as precursors in the synthesis of hydroxyapatite (HA) solutions. For the coating process, the following steps were applied; Ca(NO$_3$)$_2$·4H$_2$O and (NH$_4$)$_2$HPO$_4$ were added into DW in the separate breaker to prepare solutions with a certain molar ratio. These two solutions were mixed and stirred for 1h, and after that, ammonia solution was added into the mixed solution to adjust the pH level to around 11–12. The mixture was heated until boiling for an occurring chemical reaction, and following this step, the mixture was stirred for 24h. After 24h stirring, the solution was aged 24h and filtered. Filtered specimens were sintered at 1100°C in an electric oven (BINDER FED 115 E2) for 1h to remove excess ammonia and obtain Ca/P powders. Certain amounts of agar, DW, and Ca/P powders were agitated for the gel formation. Al2024 plates were dipped in the gel for 10min and dried at 200ºC for 30min. The dipping step was repeated several times to meet the required thickness and was finally followed by sintering at 475ºC with a ramp speed of 3°C·min^{-1} for 30min.

2.2 Characterization

The surface morphology and elemental distribution of thin film coatings were examined by scanning electron microscopy (SEM, JEOL, JSM–6335F, JSM6600) with energy dispersive spectroscopy (EDS, Oxford INCA). The phase transformation and compound formation were investigated by X-Ray diffraction (XRD, Bruker D8). XRD measurements were performed on a stage using a radiation wavelength λ=1.54056Å X-ray source with a step rate of 0.06°·s^{-1} between 20 to 80°.

2.3 Electrochemical in-vitro corrosion tests

The electrochemical *in-vitro* corrosion behavior of all groups was investigated by the potentiodynamic polarization scanning (PDS) technique. 500ml breaker was used as a cell for all measurements. The temperature of the three-electrode cell was constant at 37±1°C with the help of an automatically controlled bath in Hank's solution (SBF: Simulated body

fluid), which contained; NaCI, NaHCO₃, KCI, CaCl₂, KH₂PO₄, Glucose, and MgSO₄·7H₂O in the amount of 8.00, 0.35, 0.40, 0.14, 0.09, 1.00, and 0.20 g·L⁻¹ respectively [30]. The pH value of the solution was 7.26. A saturated Ag/AgCl, platinum wire, and specimens were used as reference, auxiliary, and working electrodes, respectively. All working electrodes prepared with cold mounting and exposed areas of specimens were 1cm². The specimens were immersed in the electrolyte until obtaining a steady open circuit potential (OCP) value. After equilibrium, The PDS experiments were carried out by increasing the potential at a scan rate of 1mV·s⁻¹ from -0.3 V vs OCP with the help of a potentiostat/galvanostat (GAMRY PCI14/750).

2.4 Scratch tests

Commonly, many researchers have used micro–scratch tests for evaluating the adhesion strength of the thin film coatings instead of pull-out tests [31–35]. The adhesion strength of specimens was determined by using a scratch tester (RST S/N:11–0175) with a pyramid diamond stylus (Rockwell Q–227 (TS ISO 3738–1)) of the 200µm radius in tests. The scratches were created on the coated surfaces by constantly increasing (30N·min⁻¹) from load 0.20 to 30.20N while the specimen was displaced at the constant speed of 10mm·min⁻¹. Total peeling–off the coatings from base materials named as critical loads [36–38]. Also, the track of the scratches micrographs was captured using a high-resolution optical microscopy device.

3 Results and discussion

Figure 1 presents XRD analysis results of uncoated and HA-coated Al2024 alloys. Characteristic peaks were found in the uncoated Al2024 alloy at 2θ degrees of 38.51° (111), 44.72° (200), 65.01° (220), and 78.30° (311), respectively (ICDD: 00-004-0787). On the other hand, XRD peaks of HA coatings synthesized using the sol-gel method were found at 2θ degrees such as 31.72°, 32.22°, 32.91°, 34.59°, and 35.13° (ICSD: 01-074-9780).
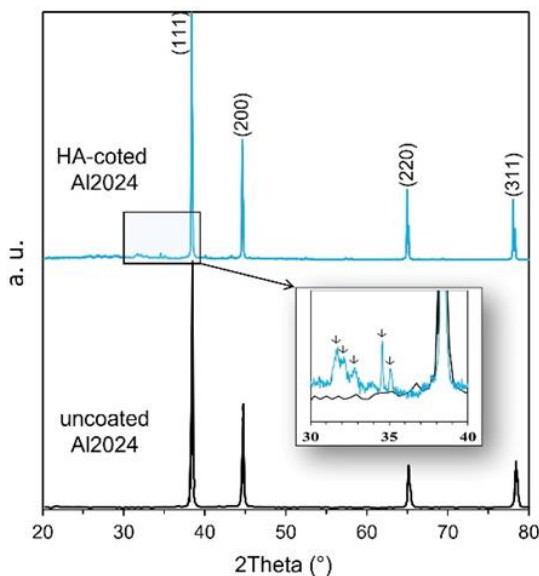

Figure 1. XRD peaks of uncoated Al2024 substrates and HA-coated (↓ HA, and sharp peaks are Al)

The absence of XRD peaks belonging to different components such as beta-tricalcium phosphate (β-TCP), and alpha-tricalcium/tetracalcium phosphate (α-TCP/TTCP) in coating suggests that the chemical stability of the coatings will be high in physiological environments [39]. In addition, it is predicted that the crystalline HA peaks obtained at 475° sintering temperature will increase the dissolution process of the coatings in the physiological environment.

Figure 2 presents SEM surface micrographs of HA-coated surfaces and EDS analysis results before the corrosion tests. As can be seen in Figure 2a, it has been determined that the Al2024 surfaces coated with HA have a nearly homogeneous surface morphology. However, considering the SEM surface morphologies at high magnifications (Figure 2b), pores in some areas along the surface were revealed. It is noteworthy that these pores are around the aggregates sized below 10µm. Various researchers have stated that HA coatings frequently encounter these accumulations [40]. It is known that these agglomerations can adversely affect the life of the coating, especially since it will increase the contact point with the environmental electrolyte during the in-body use of biomaterial coatings. However, on the other hand, it is well known that these pores will undoubtedly make a positive contribution to increasing the implant-tissue interaction [41].
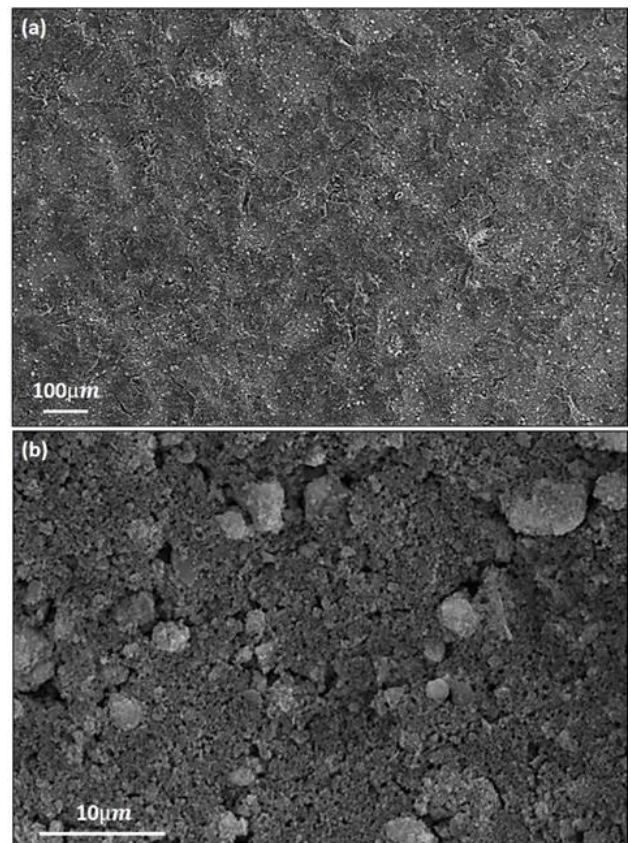

Figure 2. SEM surface morphology after HA coating of Al2024 substrates with higher magnifications

EDS results of HA-coated Al2024 alloy are given in Figure 3. As it can be understood from the elemental analysis

results of the selected region in line with the EDS mapping results, the elements that occur in the main composition of bioceramics, such as Ca and/or P, were also encountered [42]. It is predicted that these elements undoubtedly originate from the HA composition. Another element, Al, is thought that the EDS analyses may be caused by the coating not adhering to the surface locally or by micropores/pittings on the surface [43]. In addition to the EDS mapping, the areal EDS result also reflects similar results. It is thought that these relatively uncoated areas may have been the result of the sandblasting process carried out to increase the adhesion of the coating to the surface [43]. The formation of small hills (altitude difference) in some regions along the surface may cause the surface not to be completely covered homogeneously.
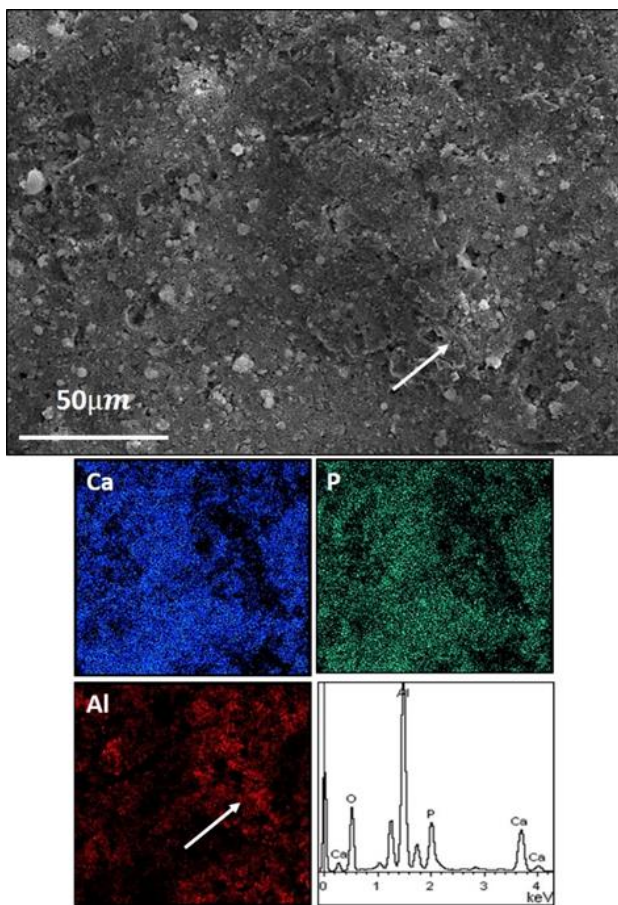

Figure 3. SEM surface morphology with EDS results after HA coating

SEM cross-sectional images of HA-coated surfaces at different scales are presented in Figures 4a and 4b, respectively. As can be seen from Figure 4a, it was determined that the roughness of the Al2024 surfaces increased after the sandblasting process. Many researchers put forth that such an increased surface roughness would play a positive role in the adhesion of the coating to the surface [43]. However, as seen in Figure 4b, local cracks were found between the coating and the Al2024 surfaces that did not extend throughout the surface. It is thought that these cracks formed during sintering rather than during the sol-gel

process [44]. It can be seen from the presence of coatings in the cross-sectional view that the surfaces immersed in the wet solution are completely covered. Predictably, these cracks are caused by the ceramic character of the coating and the metallic character of the Al2024 surfaces. It is thought that the difference between the thermal expansion coefficient of HA ($10.60 \times 106 \cdot ℃^{-1}$) and the thermal expansion coefficient of Al2024 ($22.68 \times 106 \cdot ℃^{-1}$) may be due to the different expansion rates of these two compositions during sintering and the different expansion rate during cooling [45].

On the other hand, as we obtained in our previous study [44], it has been determined that both the sintering ramp speed and the sintering temperature are highly effective on the mechanical and morphological properties of the coating in ceramic coatings made on metallic surfaces. It is seen that HA coatings have thicknesses ranging from 6.65μm to 9.10μm on average. The cross-section images also prove the presence of the Al element in the EDS analyses in Figure 2. As can be seen from Figure 2 EDS results, Al element rather than the presence of coating was found in some local areas, which supports this phenomenon.
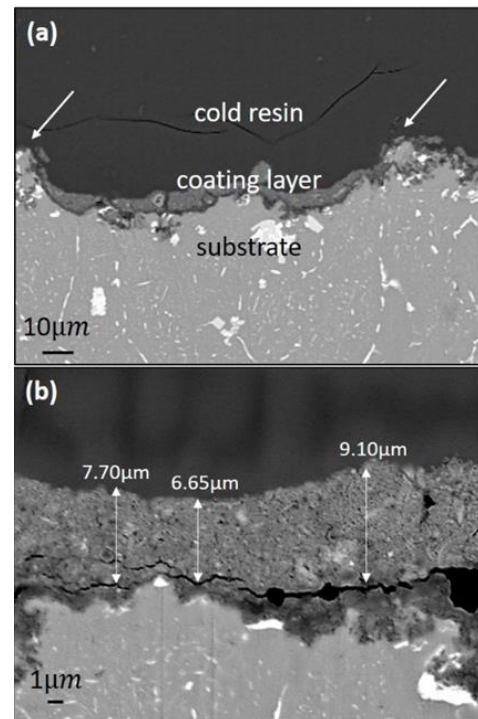

Figure 4. Cross-sectional SEM images of HA coating with different magnifications, (a) 10 μm scaled and (b) 1 μm scaled

Electrochemical corrosion results of uncoated Al2024 and HA-coated surfaces under *in-vitro* conditions are presented as PDS results in Figure 5. As can be seen from the figure, the corrosion potential (E_{corr}) value of the HA coating (-654mV) was measured slightly more than the uncoated Al2024 (-678mV) as a result of the PDS values. Important parameters collected from PDS curves are given in Table 1. In the presented parameters, another important

value for this study is undoubtedly the I_{corr} [46]. This value gives us how much the coating will corrode homogeneously per year. As a result of the corrosion rate, it can be predicted how long the HA-coated Al2024 alloys can remain in the body. This way, the corrosion current density (I_{corr}), an indication of the corrosion resistance of the samples in the electrochemical corrosion tests, was determined for uncoated Al2024 alloy was 5.260µA·cm^{-2}. The I_{corr} of HA-coated Al2024 alloy was 0.885µA·cm^{-2}, which means that HA-coated Al2024 surfaces have nearly 6 times more corrosion resistant to *in-vitro* corrosion tests in the SBF environment. As it is known, the lower the I_{corr} value, the lower the amount of current that can pass through a specific area, so the corrosion resistance of the materials will be higher [47].
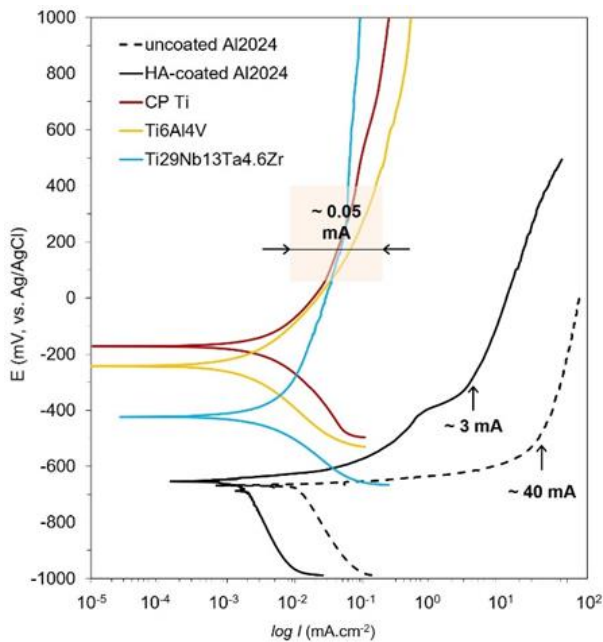

Figure 5. PDS curves of uncoated and HA-coated Al2024 substrate, with different commercial Ti alloys such as; CP Ti, Ti6Al4V, and Ti29Nb13Ta4.6Zr

Table 1. Some important corrosion parameters obtained from PDS curves

Samples	E_{corr} (mV)	I_{corr} (µA·cm^{-2})	I_{pass} (mA·cm^{-2})
Uncoated Al2024	-678	5.260	40.05
HA-coated Al2024	-654	0.885	3.15
CP Ti	-172	1.260	0.04
Ti6Al4V	-243	0.950	0.08
Ti29Nb13Ta4.6Zr	-424	1.025	0.03

Undoubtedly, this change may occur due to many different parameters (coating homogeneity, coating thickness, sintering time and temperature, etc.) that have the coating during the test. As can be seen from Figure 2 and Figure 4, the presence of pitting and local uncoated areas along the coating surface and the partially uncoated regions along the section have a negative effect on the I_{corr} value. However, it is thought that the I_{corr} value will decrease because the HA coating reduces the contact of the electrolyte with the Al2024 surface. Passivation of current density (I_{pass}), another important parameter for coatings, is that minimum current

density is required to stabilize the coating thickness within the passive range [48]. In this way, HA-coated Al2024 alloys have (40.05µA·cm^{-2}) nearly 60 times lower I_{pass} value than uncoated Al2024 alloy (3.15µA·cm^{-2}). This difference shows that a smaller current density will require the film to be formed on the Al2024 alloy with the HA coating. But on the other hand, it is seen in Figure 6 that it remains at high values (0.05µA·cm^{-2}) compared to other alloys (α, α+β, and β Ti alloys; commercial pure titanium: CP Ti, Ti6Al4V and Ti29Nb13Ta4.6Zr, respectively) currently used as biomaterials. It has been seen that even HA-coated Al2024 alloy is not suitable as a biomaterial since it cannot reach the passivation current density compared to Ti alloys. In other words, it has a very high passivation current density.

Post electrochemical corrosion SEM surface morphology of HA-coated Al2024 surfaces is presented in Figure 6. Although it can be characterized as a homogeneous corrosion mechanism on coated surfaces as seen at 500µm scale (Figure 6a), it is seen that flake-shaped coatings are removed on the surface in the magnified SEM morphology at 50µm scale (Figure 6b). It is thought that the surface morphology at high magnification may have occurred due to the agglomerations seen in Figure 2. It is thought that the region highlighted with the arrow in Figure 6b may have been detached from the surface due to the agglomeration acting more anodic than its surroundings. Another phenomenon that will be responsible for surface morphology after post-corrosion is thought that this surface morphology seen after electrochemical corrosion may be caused by the microporosities/pittings on the surface presented in Figure 4 and may also be due to the low interface strength between coating and substrate, which can be seen from the cross-sectional images (Figure 4).
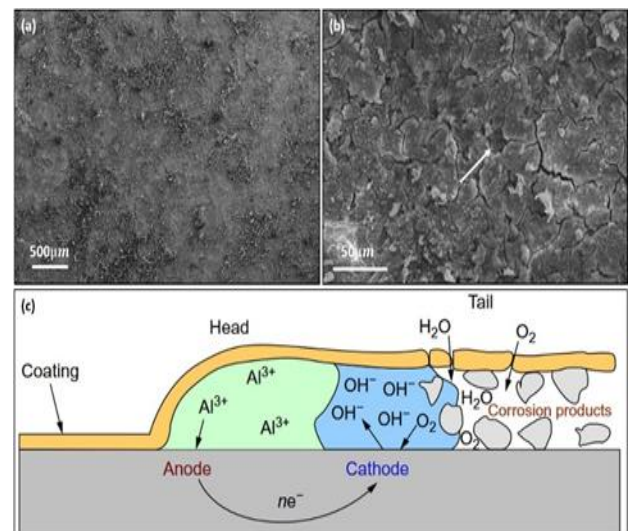

Figure 6. Post-corrosion surface morphology of HA-coated substrate with proposed filiform corrosion mechanism for Al alloys

On the other hand, during electrochemical corrosion testing of HA coatings, it was thought that it might result from the filiform corrosion mechanism, as presented in Figure 6. It is predicted that the micro-porosities on the

surface cause H_2O and O_2 ingress under the coating. A series of chemical reactions can occur beneath the coating surface, resulting in the decomposition of the coatings. By the way, with the increased polarization resistance, coating films were completely delaminated from the substrate [49].

The scratch test results of HA coatings on Al2024 surfaces are given in Figure 7. Scratch test both relationships between the friction force and coefficient obtained after the test and acoustic emission result between the coating and the surface, in which a small figure on top of the figure is presented. It has been concluded that the fact that the friction coefficient is quite wavy in the first 2mm of the scratch direction is a result of the coating surface being quite rough, as can be seen in Figure 7. On the other hand, as can be seen from the image (1st scratch picture) recorded during the test, which confirms this finding, a partial Al2024 surface is seen along the scratch trace in the first part. In contrast, a complete substrate material is seen along with the increasing normal force in the following stages (4th, 5th, and 6th scratch pictures) [42].

Moreover, with the acoustic emission values recorded during the test, it can be determined at what force range and distance the scratcher tip descends from the coating to the substrate surface [50]. As can be seen from the 3rd scratch picture, this value corresponds to approximately 12N, and it can be said that the coating is completely removed after approximately 4mm of scratch trace. This value is the coating's critical load (L_{c1}) value and represents the maximum force it can resist removing from the surface [37]. Lower critical loads (varied between 0.3 to 3.5N) were reported from another study in which HA coatings were on PCU substrates [51].
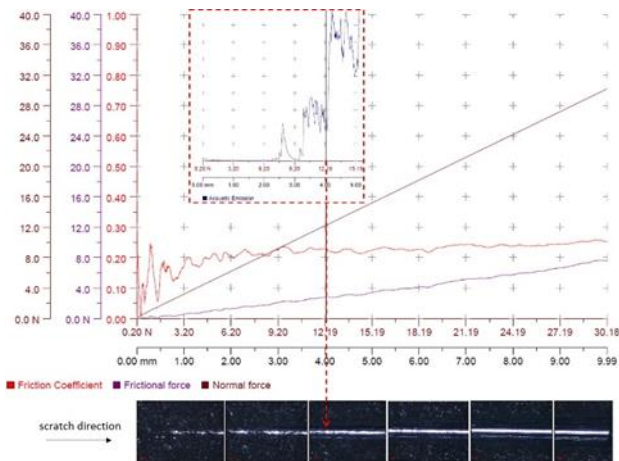

Figure 7. Scratch test results of HA coating with optical microscopy images

4 Conclusions

The biomaterial surface is in direct contact with living tissues in the body, and the tissue's response to the implant depends on the surface properties. It is well known that surface modification is significant for conventional metals and alloys (not noble in the human body) such as aluminum, magnesium, ferrous, or zinc which may cause adverse reactions to the body. In this study, the morphological, structural, mechanical, and corrosive properties of hydroxyapatite (HA) coated Al2024 alloys were investigated. Besides, the coatings' corrosion behavior was compared to the conventional implant materials under *in-vitro* conditions in simulated body fluid (SBF). While characteristic HA peaks were found in XRD analyses to confirm HA's presence on the surface, it was thought that the crystalline coating structure would increase the dissolution time in the in-body dissolution process. The SEM surface morphologies showed that the HA coating has unique microporosity. In the elemental distributions on the surfaces, Ca- and P- elements originating from HA were found in EDS analyses. Cross-sectional SEM micrographs revealed local delaminations at the interface, and it was observed that the coating was insufficient on some sharp local surface areas. It was concluded from scratch tests that HA coating on the Al2024 alloy with an adhesion force of approximately 12N would be sufficient for the in-body use of the coated metal alloys. The PDS curves showed that the Icorr value of HA-coated Al2024 alloy was lower than uncoated ones. In other words, with HA coating corrosion resistance of Al2024 alloy was increased. On the other hand, lower I_{pass} was obtained with HA coating, which means that shorten of passive film in other words, it shortened the formation time of the passive film. Although homogeneous corrosion was observed on the coating surface from the SEM surface morphologies performed after the electrochemical corrosion test, the filiform corrosion mechanism was suspected in the detailed examinations with post-SEM micrographs.

Conflict of interest

The authors declare that there is no conflict of interest.

References

[1] Y. Huang, H. Qiao, X. Nian, X. Zhang, X. Zhang, G. Song, Z. Xu, H. Zhang and S. Han, Improving the bioactivity and corrosion resistance properties of electrodeposited hydroxyapatite coating by dual doping of bivalent strontium and manganese ion. Surface and Coatings Technology, 291, 205–215, 2016. https://doi.org/10.1016/j.surfcoat.2016.02.042.

[2] A. Montenero, G. Gnappi, F. Ferrari, M. Cesari, E. Salvioli, L. Mattogno, S. Kaciulis and M. Fini, Sol-gel derived hydroxyapatite coatings on titanium substrate. Journal of Materials Science, 35, 2791–2797, 2000. https://doi.org/10.1023/A:1004738900778.

[3] J. S. Suwandi, R. E. M. Toes, T. Nikolic and B. O. Roep, Inducing tissue specific tolerance in autoimmune disease with tolerogenic dendritic cells. Clinical and Experimental Rheumatology, 33, 97–103, 2015. https://doi.org/10.1002/jbm.a.

[4] X. Liu, P. K. Chu and C. Ding, Surface modification of titanium , titanium alloys , and related materials for biomedical applications. 47, 49–121, 2005. https://doi.org/10.1016/j.mser.2004.11.001.

[5] J. B. Brunski. In Vivo Bone Response to Biomechanical Loading at the Bone/Dental-Implant

Interface, Advances in Dental Research, 13, 99-119, 1999. https://doi.org/10.1177/08959374990130123.

[6] M. Niinomi, Mechanical properties of biomedical titanium alloys. Materials Science and Engineering: A, 243, 231–236, 1998. https://doi.org/10.1016/S0921-5093(97)00806-X.

[7] M. Topuz, B. Dikici, M. Gavgalı and Y. Yılmazer, Effect of hydroxyapatite:zirconia volume fraction ratio on mechanical and corrosive properties of Ti-matrix composite scaffolds. Transactions of Nonferrous Metals Society of China, 32, 882–894, 2022. https://doi.org/10.1016/s1003-6326(22)65840-0.

[8] M. Topuz, B. Dikici, M. Gavgali and M. Kaseem, Processing of Ti/(HA+ZrO2) biocomposite and 50% porous hybrid scaffolds with low Young's modulus by powder metallurgy: Comparing of structural, mechanical, and corrosion properties. Materials Today Communications, 29, 102813, 2021. https://doi.org/10.1016/j.mtcomm.2021.102813.

[9] M. Niinomi, Recent research and development in titanium alloys for biomedical applications and healthcare goods. Science and Technology of Advanced Materials, 4, 445–454, 2003. https://doi.org/10.1016/j.stam.2003.09.002.

[10] D. Raabe, D. Ponge, P. J. Uggowitzer, M. Roscher, M. Paolantonio, C. Liu, H. Antrekowitsch, E. Kozeschnik, D. Seidmann, B. Gault, F. De Geuser, A. Deschamps, C. Hutchinson, C. Liu, Z. Li, P. Prangnell, J. Robson, P. Shanthraj, S. Vakili, C. Sinclair, L. Bourgeois and S. Pogatscher, Making sustainable aluminum by recycling scrap: The science of "dirty" alloys. Progress in Materials Science, 128, 2022. https://doi.org/10.1016/j.pmatsci.2022.100947.

[11] N. M. Siddesh Kumar, Dhruthi, G. K. Pramod, P. Samrat and M. Sadashiva, A Critical Review on Heat Treatment of Aluminium Alloys. Materials Today: Proceedings, 58, 71–79, 2022. https://doi.org/10.1016/j.matpr.2021.12.586.

[12] M. Zarka, B. Dikici, M. Niinomi, K. V. Ezirmik, M. Nakai and M. Kaseem, The Ti3.6Nb1.0Ta0.2Zr0.2 coating on anodized aluminum by PVD: A potential candidate for short-time biomedical applications. Vacuum, 192, 110450, 2021. https://doi.org/10.1016/j.vacuum.2021.110450.

[13] P. H. Setyarini, F. Gapsari and Purnomo, Fabrication of Aluminum Using Casting Method Made for Anodizing Process on Biomaterial Applications. IOP Conference Series: Materials Science and Engineering, 494, 2019. https://doi.org/10.1088/1757-899X/494/1/012063.

[14] Ž. Petrović, A. Šarić, I. Despotović, J. Katić and M. Petković, Aluminum in dental implants: how to reduce a potential risk to patient´s health? Proc. 1st Corros. Mater. Degrad. Web Conf. (Basel, Switzerland: MDPI, 2021), p. 9933. https://doi.org/10.3390/CMDWC2021-09933.

[15] C. Leyens and M. Peters, Titanium and its Alloys for Medical Applications. Titan. Titan. Alloy, pp. xix, 423, 2003. https://doi.org/10.1002/3527602119.

[16] O. Prokopiev and I. Sevostianov, Dependence of the mechanical properties of sintered hydroxyapatite on the sintering temperature. Materials Science and Engineering A, 431, 218–227, 2006. https://doi.org/10.1016/j.msea.2006.05.158.

[17] H. W. Kim, S. Y. Lee, C. J. Bae, Y. J. Noh, H. E. Kim, H. M. Kim and J. S. Ko, Porous ZrO2 bone scaffold coated with hydroxyapatite with fluorapatite intermediate layer. Biomaterials, 24, 3277–3284, 2003. https://doi.org/10.1016/S0142-9612(03)00162-5.

[18] I. Bogdanoviciene, A. Beganskiene, K. Tõnsuaadu, J. Glaser, H.-J. Meyer and A. Kareiva, Calcium hydroxyapatite, Ca10(PO4)6(OH)2 ceramics prepared by aqueous sol–gel processing. Materials Research Bulletin, 41, 1754–1762, 2006. https://doi.org/10.1016/j.materresbull.2006.02.016.

[19] S. J. Kalita, A. Bhardwaj and H. A. Bhatt, Nanocrystalline calcium phosphate ceramics in biomedical engineering. Materials Science and Engineering C, 27, 441–449, 2007. https://doi.org/10.1016/j.msec.2006.05.018.

[20] M. Enayati-Jazi, M. Solati-Hashjin, A. Nemati and F. Bakhshi, Synthesis and characterization of hydroxyapatite/titania nanocomposites using in situ precipitation technique. Superlattices and Microstructures, 51, 877–885, 2012. https://doi.org/10.1016/j.spmi.2012.02.013.

[21] L. Zhou, G.-H. Lü, F.-F. Mao and S.-Z. Yang, Preparation of biomedical Ag incorporated hydroxyapatite/titania coatings on Ti6Al4V alloy by plasma electrolytic oxidation. Chinese Physics B, 23, 035205, 2014. https://doi.org/10.1088/1674-1056/23/3/035205.

[22] A. Balamurugan, G. Balossier, S. Kannan, J. Michel, J. Faure and S. Rajeswari, Electrochemical and structural characterisation of zirconia reinforced hydroxyapatite bioceramic sol–gel coatings on surgical grade 316L SS for biomedical applications. Ceramics International, 33, 605–614, 2007. https://doi.org/10.1016/j.ceramint.2005.11.011.

[23] B. Y. Chou and E. Chang, Microstructural characterization of plasma-sprayed hydroxyapatite-10 wt% ZrO2 composite coating on titanium. Biomaterials, 20, 1823–1832, 1999. https://doi.org/10.1016/S0142-9612(99)00078-2.

[24] K. Im, M. Kim, D. Kang, K. Kim, K. Kim and Y. Lee, Hydroxyapatite / Titania Hybrid Coatings on Titanium by Sol-Gel Process. Biomaterials Research, 10, 224–230, 2006.

[25] R. R. Kumar and M. Wang, Functionally graded bioactive coatings of hydroxyapatite / titanium oxide composite system. Materials Letters, 55, 133–137, 2002. https://doi.org/10.1016/S0167-577X(01)00635-8.

[26] Y. W. Gu, K. a. Khor, D. Pan and P. Cheang, Activity of plasma sprayed yttria stabilized zirconia reinforced hydroxyapatite/Ti-6Al-4V composite coatings in simulated body fluid. Biomaterials, 25, 3177–3185i,

2004.
https://doi.org/10.1016/j.biomaterials.2003.09.101.

[27] Y. T. Zhao, Z. Zhang, Q. X. Dai, D. Y. Lin and S. M. Li, Microstructure and bond strength of HA(+ZrO2+Y2O3)/Ti6Al4V composite coatings fabricated by RF magnetron sputtering. Surface and Coatings Technology, 200, 5354–5363, 2006. https://doi.org/10.1016/j.surfcoat.2005.06.010.

[28] D. H. He, P. Wang, P. Liu, X. K. Liu, F. C. Ma and J. Zhao, HA coating fabricated by electrochemical deposition on modified Ti6Al4V alloy. Surface and Coatings Technology, 277, 203–209, 2015. https://doi.org/10.1016/j.surfcoat.2015.07.038.

[29] S. Sonmez, B. Aksakal and B. Dikici, Corrosion protection of AA6061-T4 alloy by sol–gel derived micro and nano-scale hydroxyapatite (HA) coating. Journal of Sol-Gel Science and Technology, 63, 510–518, 2012. https://doi.org/10.1007/s10971-012-2813-8.

[30] X. Liu, J. Sun, F. Zhou, Y. Yang, R. Chang, K. Qiu, Z. Pu, L. Li and Y. Zheng, Micro-alloying with Mn in Zn-Mg alloy for future biodegradable metals application. Materials and Design, 94, 95–104, 2016. https://doi.org/10.1016/j.matdes.2015.12.128.

[31] X. Nie, A. Leyland and A. Matthews, Deposition of layered bioceramic hydroxyapatite/TiO2 coatings on titanium alloys using a hybrid technique of micro-arc oxidation and electrophoresis. Surface and Coatings Technology, 125, 407–414, 2000. https://doi.org/10.1016/S0257-8972(99)00612-X.

[32] H. Farnoush, J. Aghazadeh Mohandesi and H. Çimenoğlu, Micro-scratch and corrosion behavior of functionally graded HA-TiO2 nanostructured composite coatings fabricated by electrophoretic deposition. Journal of the Mechanical Behavior of Biomedical Materials, 46, 31–40, 2015. https://doi.org/10.1016/j.jmbbm.2015.02.021.

[33] K. H. Im, S. B. Lee, K. M. Kim and Y. K. Lee, Improvement of bonding strength to titanium surface by sol-gel derived hybrid coating of hydroxyapatite and titania by sol-gel process. Surface and Coatings Technology, 202, 1135–1138, 2007. https://doi.org/10.1016/j.surfcoat.2007.07.081.

[34] S. Zhang, Z. Xianting, W. Yongsheng, C. Kui and W. Wenjian, Adhesion strength of sol-gel derived fluoridated hydroxyapatite coatings. Surface and Coatings Technology, 200, 6350–6354, 2006. https://doi.org/10.1016/j.surfcoat.2005.11.033.

[35] D. Sidane, D. Chicot, S. Yala, S. Ziani, H. Khireddine, A. Iost and X. Decoopman, Study of the mechanical behavior and corrosion resistance of hydroxyapatite sol-gel thin coatings on 316 L stainless steel pre-coated with titania film. Thin Solid Films, 593, 71–80, 2015. https://doi.org/10.1016/j.tsf.2015.09.037.

[36] H. U. Lee, Y. S. Jeong, S. Y. Park, S. Y. Jeong, H. G. Kim and C. R. Cho, Surface properties and cell response of fluoridated hydroxyapatite/TiO2 coated on Ti substrate. Current Applied Physics, 9, 528–533, 2009. https://doi.org/10.1016/j.cap.2008.03.020.

[37] E. Mohseni, E. Zalnezhad and A. R. Bushroa, Comparative investigation on the adhesion of hydroxyapatite coating on Ti–6Al–4V implant: A review paper. International Journal of Adhesion and Adhesives, 48, 238–257, 2014. https://doi.org/10.1016/j.ijadhadh.2013.09.030.

[38] K. Im, S. Lee, K. Kim and Y. Lee, Improvement of bonding strength to titanium surface by sol – gel derived hybrid coating of hydroxyapatite and titania by sol – gel process. 202, 1135–1138, 2007. https://doi.org/10.1016/j.surfcoat.2007.07.081.

[39] H. W. Kim, H. E. Kim, V. Salih and J. C. Knowles, Hydroxyapatite and titania sol-gel composite coatings on titanium for hard tissue implants; mechanical and in vitro biological performance. Journal of Biomedical Materials Research - Part B Applied Biomaterials, 72, 1–8, 2005. https://doi.org/10.1002/jbm.b.30073.

[40] O. Yigit, B. Dikici, T. C. Senocak and N. Ozdemir, One-step synthesis of nano-hydroxyapatite/graphene nanosheet hybrid coatings on Ti6Al4V alloys by hydrothermal method and their in-vitro corrosion responses. Surface and Coatings Technology, 394, 125858, 2020. https://doi.org/10.1016/j.surfcoat.2020.125858.

[41] M. Topuz, B. Dikici and M. Gavgali, Titanium-based composite scaffolds reinforced with hydroxyapatite-zirconia: Production, mechanical and in-vitro characterization. Journal of the Mechanical Behavior of Biomedical Materials, 118, 104480, 2021. https://doi.org/10.1016/j.jmbbm.2021.104480.

[42] B. Dikici, M. Niinomi, M. Topuz, S. G. Koc and M. Nakai, Synthesis of biphasic calcium phosphate (BCP) coatings on β–type titanium alloys reinforced with rutile-TiO2 compounds: adhesion resistance and in-vitro corrosion. Journal of Sol-Gel Science and Technology, 87, 713–724, 2018. https://doi.org/10.1007/s10971-018-4755-2.

[43] M. Topuz and B. Dikici, Two simple methods for surface modification of lithium disilicate dental blocks with hydroxyapatite. Research on Engineering Structures and Materials, 2019. https://doi.org/10.17515/resm2019.132me0506tn.

[44] B. Dikici, M. Niinomi, M. Topuz, Y. Say, B. Aksakal, H. Yilmazer and M. Nakai, Synthesis and Characterization of Hydroxyapatite/TiO2 Coatings on the β-Type Titanium Alloys with Different Sintering Parameters using Sol-Gel Method. Protection of Metals and Physical Chemistry of Surfaces, 54, 457–462, 2018. https://doi.org/10.1134/S2070205118030255.

[45] H. Miyazaki, I. Ushiroda, D. Itomura, T. Hirashita, N. Adachi and T. Ota, Thermal expansion of hydroxyapatite between - 100 °C and 50 °C. Materials Science and Engineering C, 29, 1463–1466, 2009. https://doi.org/10.1016/j.msec.2008.12.001.

[46] F. Songur, B. Dikici, M. Niinomi and E. Arslan, The plasma electrolytic oxidation (PEO) coatings to enhance in-vitro corrosion resistance of Ti–29Nb–13Ta–4.6Zr alloys: The combined effect of duty cycle and the deposition frequency. Surface and Coatings

Technology, 374, 345–354, 2019. https://doi.org/10.1016/j.surfcoat.2019.06.025.

[47] O. Yigit, B. Dikici, N. Ozdemir, E. Arslan, T. C. Senocak and N. Ozdemir, Plasma electrolytic oxidation of Ti-6Al-4V alloys in nHA/GNS containing electrolytes for biomedical applications: The combined effect of the deposition frequency and GNS weight percentage. Surface and Coatings Technology, 32, 127139, 2021. https://doi.org/10.1007/s10856-021-06514-w.

[48] H. A. Hameed, H. A. Hasan and M. K. Alam, Evaluation of Corrosion Behavior by Measuring Passivation Current Density of Dental Implant Coated with Bioceramic Materials. BioMed Research International, 2021. https://doi.org/10.1155/2021/9934073.

[49] K. A. Yasakau, M. L. Zheludkevich and M. G. S. Ferreira, Role of intermetallics in corrosion of aluminum alloys. Smart corrosion protection, Elsevier Ltd., 2018. https://doi.org/10.1016/B978-0-85709-346-2.00015-7.

[50] G. E. L. Processing, Handbook of Sol-Gel Science and Technology: Processing, Characterization and Applications, Volumes I−III Set edited by Sumio Sakka (Professor Emeritus of Kyoto University). Kluwer Academic Publishers: Boston, Dordrecht, London. 2005. lx + 1980 pp. 1500. Journal of the American Chemical Society, 127, 6135–6135, 2005. https://doi.org/10.1021/ja041056m.

[51] D. Barnes, S. Johnson, R. Snell and S. Best, Using scratch testing to measure the adhesion strength of calcium phosphate coatings applied to poly(carbonate urethane) substrates. Journal of the Mechanical Behavior of Biomedical Materials, 6, 128–138, 2012. https://doi.org/10.1016/j.jmbbm.2011.10.010.